Determination of Total Absorption of Na $3S \rightarrow nP$ Transitions for $5 \leqq n \leqq 28$

L. Dressler, W. Behmenburg, and J. Uhlenbusch *

Physikalisches Institut, Universität Düsseldorf

Z. Naturforsch. **33 a**, 432–438 (1978) ; received January 27, 1978

Total absorption measurements of Na $3S \rightarrow nP$ transitions up to a main quantum number $n=28$ have been performed at Na number densities in the range $\approx 10^{16}-10^{17}$ cm^{-3} and temperatures $\approx 700-800$ K. A heat pipe oven has been applied as an absorption tube in a single beam optical arrangement; experiment and data acquisition have been controlled by a computer. The results are compared with calculations using special assumptions with respect to line broadening mechanisms. The effect of binary and three-body collisions on total absorption is studied in detail. Within the pressure and main quantum number range investigated here a transition between the two types of interaction was demonstrated.

1. Introduction

Very recently atomic highly excited states close to the series limits as well as autoionizing states have become the object of many research activities [1]. These have been much stimulated by the advent of laser high resolution Doppler free spectroscopy. Since the transitions involved are generally very weak, besides strong excitation, sufficiently large metal vapour densities are required to obtain spectra. For this purpose a heat pipe oven [2] offers itself, where number densities ranging from 10^{15} to 10^{18} cm^{-3} may be generated by varying the buffer gas pressure. Since in a heat pipe oven absorbing layers of well defined lengths can be produced, also absolute absorption coefficients and thus f-values may be determined. Finally the quoted range of densities yields the possibility of studying nonlinear optical effects as well as collisional broadening of spectral lines and other relaxation phenomena.

In order to demonstrate the applicability of the heat pipe oven to these kinds of studies, a computer controlled absorption experiment has been carried out. The total absorption of Na principal series lines $3S \rightarrow nP$ for $5 \leqq n \leqq 25$ has been measured at Na number densities 1.22×10^{16} and 1.16×10^{17} cm^{-3} corresponding to temperatures of 701 K and 813 K, respectively. Observations have been made using a grating monochromator of medium resolution at an apparatus width of ≈ 0.3 Å. The experimental results have been compared with calculations using special assumptions with respect to the line profile.

* Requests for reprints to Prof. J. Uhlenbusch, Physikalisches Institut, Universität Düsseldorf, Universitätsstr. 1, D-4000 Düsseldorf.

2. Calculation of Total Absorption

For an isolated line the total absorption or equivalent width of an absorbing layer is defined by

$$W_\nu = \int \mathrm{d}\nu \, \{1 - \exp[-k(\nu) l]\} . \tag{1}$$

The frequency dependent absorption coefficient $k(\nu)$ may be represented by

$$k(\nu) = \pi r_0 c N_\mathrm{A} f P(\nu) , \tag{2}$$

where r_0 = classical electron radius, c = velocity of light, N_A = number density of absorbing atoms, f = absorption oscillator strength of the transition; $P(\nu)$ is the normalized line shape function. For the realistic case under study of a Na-transition of type $3S \rightarrow nP$ consisting of a multiplet of fine and hyperfine structure components i (see Section 2.3) the generalized expression for the total absorption reads

$$W_{\nu,n} = \int \mathrm{d}\nu \, \{1 - \exp [\sum_i k_{n,i}(\nu - \nu_i) l]\} \tag{3}$$

with $k_{n,i}(\nu - \nu_i) = \pi r_0 c N_\mathrm{A} f_{n,i} P_{n,i}(\nu - \nu_i)$.

It should be noted that the measured value of W_ν is independent of the instrumental profile.

2.1. Line Profiles

The line profiles $P_{n,i}(\nu)$ could not be determined in this experiment because of insufficient resolution of the spectrograph. Therefore, they had to be calculated on the basis of line broadening theory using certain approximations.

Generally $P_{n,i}(\nu)$ results from the superposition of various broadening mechanisms: radiation damping, Doppler effect by thermal motion and collisions.

The effect of radiation damping is described by a Lorentzian function of full halfwidth

$$\Delta\nu_N = \frac{4\pi}{3} r_0 \frac{c}{\nu_0^2} \tag{4}$$

where ν_0 is the center frequency of the line, r_0 = classical electron radius.

Doppler broadening is represented by the Gaussian function of full halfwidth

$$\Delta\nu_D = \frac{2\sqrt{\ln 2}}{c}\sqrt{\frac{2RT}{M}}\nu_0, \tag{5}$$

where R is the gas constant, M the reduced mass, and T the temperature. For T experimental values were used *.

The collisional part of $P_{n,i}(\nu)$ is more complicated. The region near the line center may, under the present experimental conditions, be assumed to be Lorentzian shaped, independently of the nature of interaction; however the halfwidths and the shape of the wings strongly depend on the interaction potential [4].

For the lower lying excited states both resonance interaction $\sim r^{-3}$ (r internuclear distance) and Van der Waals interaction $\sim r^{-6}$ have to be considered. For highly excited states, on the other hand, the perturbation is governed by a three-body interaction, namely the highly excited valence electron in the Coulomb field of the parent ion and the attracting short range potential of the perturbing atom.

According to the impact approximation of collisional line broadening theory the Lorentzian width is, in case of r^{-3} interaction, given by [5]

$$\Delta\nu_3(n) = 0.153\, r_0\, c^2 \frac{f}{\nu_0}\sqrt{\frac{g_2}{g_1}}\, N_p \tag{8}$$

(f = oscillator strength, $g_{1,2}$ = statistical weights, N_p = perturber number density).

The f-values needed for the calculation of $\Delta\nu_3$ were taken from tables [6]; for $n>14$ they were calculated with sufficient accuracy according to $f = 0.0522\, n^{*-3}$.

In case of r^{-6} interaction one obtains [7]

$$\Delta\nu_6(n) = 2.71\left(\frac{C_6(n)}{h}\right)^{2/5}\bar{v}^{3/5} N_p, \tag{9}$$

where $\bar{v}$ is the mean relative velocity; the Van der Waals constant is calculated with the use of the expression

$$C_6(n) = e^2\,\alpha(\overline{r_i^2} - \overline{r_f^2}), \tag{10}$$

where $\overline{r_i^2}$, $\overline{r_f^2}$ are the quantum mechanical average values of the atomic radii for the lower and upper level of the transition respectively, and α is the perturber polarizability. For $\overline{r^2}$ we use the approximative expression [7]

$$\overline{r^2} = \tfrac{1}{2} a_0^2\, n^{*2}\,[5\, n^{*2} + 1 - 3\, l(l+1)], \tag{11}$$

where a_0 is the Bohr radius. For α of Na the value 20 Å^3 was used [8].

At small n, especially for the resonance transition, $\Delta\nu_3$ and $\Delta\nu_6$ are of the same order of magnitude. With increasing n, however, $\Delta\nu_3$ decreases $\sim n^{*-3}$ whereas $\Delta\nu_6$ increases $\sim n^{*4}$, so that for $n \geqq 5$, $\Delta\nu_3$ is small compared to $\Delta\nu_6$ (see Table 1).

Table 1. Halfwidths and oscillator strengths for Na $3S \rightarrow n\,P$ transitions. $N_p = 1.26$ E17 cm^{-1}; $T = 813$ K; $\Delta\nu_\infty = 1.46$ E9 Hz; the $\Delta\nu_3$-values refer to the $P_{3/2}$-components.

n	f	$\Delta\nu_D$/Hz	$\Delta\nu_3$/Hz	$\Delta\nu_6$/Hz	$\Delta\nu_{3+6}$/Hz
4	1.42 E-2	2.32 E9	9.92 E7	3.02 E8	3.07 E8
5	2.21 E-3	2.69 E9	1.33 E7	4.93 E8	4.93 E8
6	7.30 E-4	2.68 E9	4.14 E6	7.09 E8	7.09 E8
7	3.61 E-4	2.96 E9	1.98 E6	9.49 E8	9.50 E8
8	1.92 E-4	3.02 E9	1.03 E6	1.21 E9	1.21 E9
9	1.15 E-4	3.05 E9	6.11 E5	1.50 E9	1.50 E9
10	7.70 E-5	3.08 E9	4.06 E5	1.81 E9	1.81 E9
11	5.30 E-5	3.10 E9	2.77 E5	2.14 E9	2.14 E9
12	3.92 E-5	3.11 E9	2.04 E5	2.49 E9	2.49 E9
13	3.03 E-5	3.12 E9	1.57 E5	2.85 E9	2.85 E9
14	2.31 E-5	3.13 E9	1.20 E5	3.24 E9	3.24 E9
15	1.84 E-5	3.14 E9	9.54 E4	3.65 E9	3.65 E9
16	1.50 E-5	3.14 E9	7.76 E4	4.07 E9	4.07 E9
17	1.24 E-5	3.15 E9	6.39 E4	4.51 E9	4.51 E9
18	1.04 E-5	3.15 E9	5.33 E4	4.96 E9	4.96 E9
19	8.74 E-6	3.16 E9	4.49 E4	5.44 E9	5.44 E9
20	7.44 E-6	3.16 E9	3.82 E4	5.93 E9	5.93 E9
21	6.38 E-6	3.16 E9	3.28 E4	6.43 E9	6.43 E9
22	5.52 E-6	3.16 E9	2.83 E4	6.95 E9	6.95 E9
23	4.80 E-6	3.16 E9	2.46 E4	7.48 E9	7.48 E9
24	4.21 E-6	3.17 E9	2.16 E4	8.03 E9	8.03 E9
25	3.71 E-6	3.17 E9	1.90 E4	8.59 E9	8.59 E9
26	3.28 E-6	3.17 E9	1.68 E4	9.17 E9	9.17 E9
27	2.92 E-6	3.17 E9	1.50 E4	9.76 E9	9.76 E9
28	2.61 E-6	3.17 E9	1.34 E4	1.04 E10	1.04 E10

* The dependence of line frequency $\nu_0 \equiv \nu_n$ on quantum number n is represented by the Rydberg-Ritz formula [3]

$$\nu_n = \nu_i - R_\infty\, n_l^{*-2} \tag{6}$$

with $\nu_i = E_i/h$, E_i = ionization energy and

$$n_l^* = n - \alpha(l) - \beta(l)\, n^{-2}, \tag{7}$$

where n_l^* is the effective quantum number, called n^* in the following.

Calculations have been performed with $E_i = 5.144$ eV, $R_\infty = 3.2898 \times 10^{15}$ Hz, $\alpha(1) = 0.8534$, $\beta(1) = 0.2756$.

It should be noted that the halfwidth $\Delta\nu_{3+6}$, resulting from the combined resonance- and Van der Walls-interaction $V(r) = -C_3 r^{-3} - C_6 r^{-6}$, is generally not equal to $\Delta\nu_3 + \Delta\nu_6$. We have therefore calculated $\Delta\nu_{3+6}$ correctly from theory [9]. For $n \geqq 5$ it turned out, however, that $\Delta\nu_{3+6} \approx \Delta\nu_3 + \Delta\nu_6$ up to a high degree of accuracy (see Table 1).

With increasing n, i. e. increasing atomic radius, binary interaction changes over into three-body-interaction. For very large n, theory [10] yields for the halfwidth

$$\Delta\nu_\infty = \frac{5}{8}\left(\frac{4\pi^2 e^2}{h}\right)^{2/3} \alpha^{2/3}\, \bar{v}^{1/3}\, N_p\,. \tag{12}$$

The boundary between the validity regions of the two types of interaction may be characterized by that $n_L{}^*$ where the atomic radius $\bar{r}_f$ equals the average internuclear distance $r_0 = [(4\pi/3)N]^{2/3}$. Using (11), $n_L{}^*$ is obtained from

$$\frac{a_0}{\sqrt{2}}\, n_L{}^* \left[5\, n_L{}^{*2} + 1 - 31\,(l+1)\right]^{1/2} = \left(\frac{4\pi}{3} N_p\right)^{-1/3}. \tag{13}$$

2.2. Convolution of the Profiles

For calculation of the total line shape $P_{n,i}(\nu)$ the individual functions representing the various broadening mechanisms have been folded. In particular, the collisional Lorentz profile was folded into the Doppler profile resulting in the well known Voigt function. This widely-practiced procedure assumes collision- and Doppler broadening to be independent processes. One should note, however, that collisions generally change the velocity of the active atom and may therefore cause the resulting profile to deviate from the Voigt type [11].

In the numerical integration of the folding integral

$$G(\nu') = \int_{-\infty}^{+\infty} f(\nu)\, g(\nu' - \nu)\, \mathrm{d}\nu \tag{14}$$

the Doppler profile was substituted for $f(\nu)$, the Lorentz profile for $g(\nu)$. Integration using Simpson's rule was performed in the limits $(-5\,\Delta\nu_D,\ 5\,\Delta\nu_D)$, the stepwidth h of integration was chosen to be $h = 0.1\,\Delta\nu_D$. The contribution of the interval $-h/2 \leqq \nu' - \nu \leqq h/2$ to $G(\nu')$ has been approximated by the integral $\int_{-h/2}^{+h/2} g(\nu)\, \mathrm{d}\nu$. Errors arising in this procedure have been discussed in detail elsewhere [12].

2.3. Line Structure

For the calculation of total absorption in addition to line broadening the fine and hyperfine structure splitting of the unperturbed atom have to be considered.

The frequency difference of the two fine structure components was calculated from [13]

$$\Delta\nu_{n,l} = \frac{\alpha^2}{l(l+1)}\, Z_a{}^2\, Z_i{}^2\, R_y\, n^{*-3} = \frac{C}{n^{*3}} \tag{15}$$

(α fine structure constant, Z_a effective nuclei charge, R_y Rydberg constant).

The factor C was determined from the experimental value of $\Delta\nu_{3,1} = 554 \times 10^9$ Hz [6].

With respect to hyperfine structure, only the splitting of the 3S level was taken into account. For calculation the experimental value 1771.6 MHz [14] was used, which is of the order of the Doppler width. Compared to this, the splitting of the $n\,P$ levels, which decreases proportional to n^{*-3}, may be neglected.

The relative oscillator strengths of the fine and hyperfine components were obtained from the Clebsch-Gordon coefficients.

3. Experimental

3.1. Optical Arrangement

Figure 1 shows the optical set up. The circularly shaped anode of a deuterium lamp D_L was telecentrically imaged onto the entrance slit of the monochromator MC. The heat pipe oven was placed within the parallel part of the ray path, as was the computer-controlled chopper U which interrupted the light beam for dark current measurements. The aperture of the lens L_2, $\approx 1/20$, was approximately adjusted to that of the monochromator, $\approx 1/30$. The apparatus width of the latter was ≈ 0.3 Å. For light detection an RCA 1 P28 Multiplier with Keithley 410 A Current Amplifier was used.

3.2. Heat Pipe Oven

The heat pipe oven used in this experiment consisted of a 1 m length of 4541 stainless steel pipe, 5 cm in diameter and 1.5 mm in wall thickness. The wick was made of screen of the same material (0.1 mm wires, 0.25 mm mesh) rolled into a 3 layered tube.

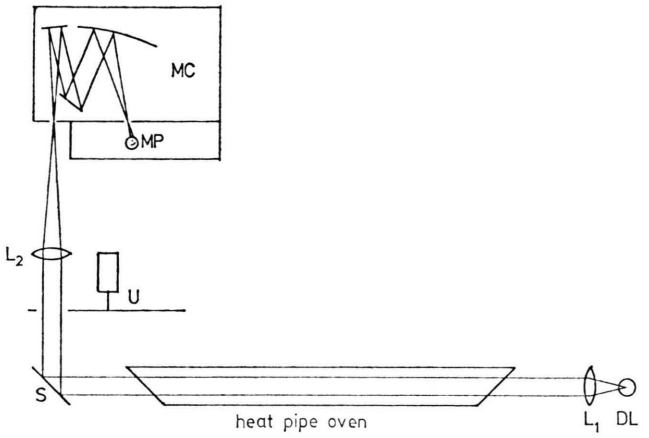

Fig. 1. Optical arrangement of the experiment.

The heat was supplied by a 40 mm long electrical heating coil at the center of the pipe. The heat was dissipated by 2 symmetrical watercooled coils. Heat insulation, sufficient for actual operation temperatures below 550 °C, was effected by means of several layers of ceramic fibre.

In order to operate the oven, the pipe was filled with about 50 gr of Na together with Ar as buffer gas at a suitable pressure. Several measures were necessary for clean preparation and to achieve complete wetting of the wick with the liquid Na; they are reported in Reference [12].

For measurement of the axial temperature profile, Ni – CrNi thermocouples were spot-welded onto the outer tube wall at intervals of 20 mm. In order to keep the length of the absorbing layer constant during the time of measurement, the heating power had to be regulated. This was achieved via temperature control at a point located in the wing of the temperature profile.

Figure 2 shows typical temperature shapes for various values of the heating power P. In agreement with theory [15] a plateau is observed, the length

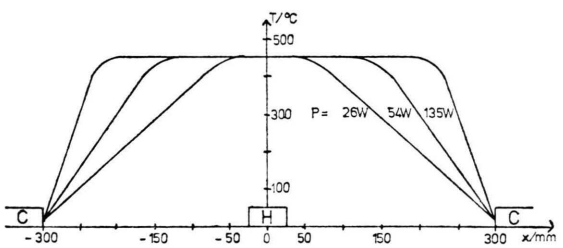

Fig. 2. Experimental temperature profiles at the heat pipe oven.

of which increases with P. The temperature decrease towards the water cooling coils is nearly linear according to constant heat conductivity on the pipe walls.

3.3. *Computer Controlling the Experiment*

The experiment was computer-controlled by applying a computer SPC-16 together with a teletype ASR-33 of General Automation. Controlled parts of the system were the analog-digital converter for data acquisition and, via step motors, the wavelength drive of the monochromator and the chopper for dark current measurements (Figure 3).

For the monochromator a step motor RDM 596/50 of Berger was used, with a step angle of 0.72°, corresponding to a wavelength setting of 0.012 Å. The relaxation time of the monochromator after each step was less than 0.2 s; a time interval between motor control and data acquisition of 0.5 s was programmed. For fast runs a rate of up to 80 steps per second, corresponding to 0.96 Å/s, was attainable.

Connected to the step motor Knab KS 042.3.12 for the chopper was a sector disc with two antipodal 90° segments. The relaxation time of the chopper was about 0.5 s.

At the beginning of each spectrum scan 50 values for the dark current were picked up, thereafter the sector disk was turned, so that the light beam could pass through. Next, the wavelength position of the monochromator was changed step by step and an intensity measurement performed each time. After 300 measurements (at lower series members) or 1800 measurements (at closely lying lines near the series limit) the dark current was measured again. Between the far apart lying lower series members the wavelength was changed at the maximum rate of 0.96 Å/s.

3.4. *Data Acquisition*

Figure 4 shows schematically the arrangement used for data acquisition. The multiplier 1 P28 was operated with a power supply of 1 kV. A preamplifier converted current signals of the order of 10^{-8} A into proportional voltage signals of the order of 1 V. The dark current of the multiplier was about 6×10^{-10} A.

For long time control (drift of the background intensity, position of wavelength) the signal was displayed on a $x-t$ chart recorder, for short time

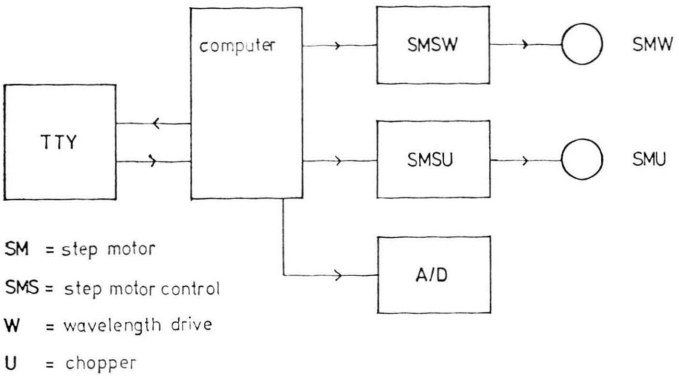

Fig. 3. Scheme for computer controlling the experiment.

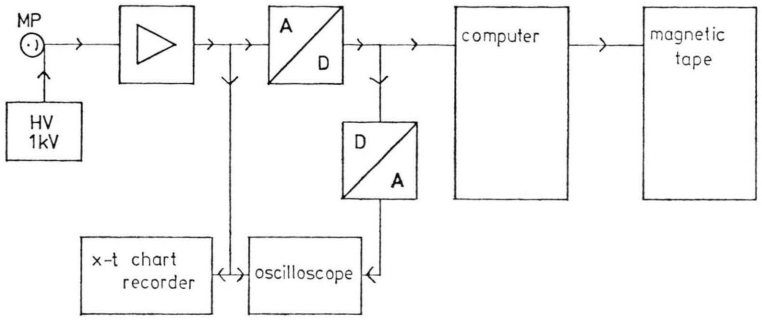

Fig. 4. Scheme for data aquisition.

control (noise peaks) on an oscilloscope. For processing by the computer the signal was then transferred to a A/D converter. Because of its operation at small modulation degree the resolution was only about 5.7 bit (50 steps). This appeared to be sufficient, however, since even after conversion the multiplier noise was still noticeable. For control of the A/D converter the digital value was fed back into a D/A converter and the output voltage was compared with the input voltage on the oscilloscope.

In order to eliminate noise 20480 measurements were taken at each step of the spectrum and then averaged by the computer. Due to the short time of 60 μs between two measurements and the long total measuring time of 1.2 s also noise of mains frequency could largely be eliminated. 2000 measuring values were stored by the computer and transferred to the tape before continuation of measurement. Processing of the averaged values was effected with an accuracy of 10 bit (1‰).

4. Results and Conclusions

Figure 5 shows plots of the equivalent width W_λ vs. quantum number n, measured at two number densities N_p differing by about a factor of 10. The relatively large error bounds of the high density measurement at $n=5$ are due to Na_2 band structure superimposed on the line profile. The observed decrease of $W_\lambda(n)$ is essentially due to the decrease of $f(n) \sim n^{*-3}$ and the change of the line shape wih n.

It is to be noted that for all n the observed increase of W_λ with N_p is considerably larger than $\sim \sqrt{N_p}$. This is to be expected for very large optical depths, if the asymmetric wings contribute considerably to the integrated absorption. Actual asymmetries in the transmission profiles have been observed at small n as well as indications of asymmetries even up to the largest n studied, in which case the measured profiles are dominated by the symmetric apparatus profile.

For comparison of experiment with theory $W_\lambda(n)$ was calculated for two types of interaction: 1) binary interaction, described by $V(r) = -C_3 r^{-3} - C_6 r^{-6}$ with resulting collisional halfwidths taken from Table 1; 2) three-body-interaction, where the halfwidth was calculated from Equation (12). For simplicity the collisional line profiles were assumed throughout to be purely Lorentzian. In addition to systematic errors, which may arise from this assumption, uncertainties in the f-values of up to

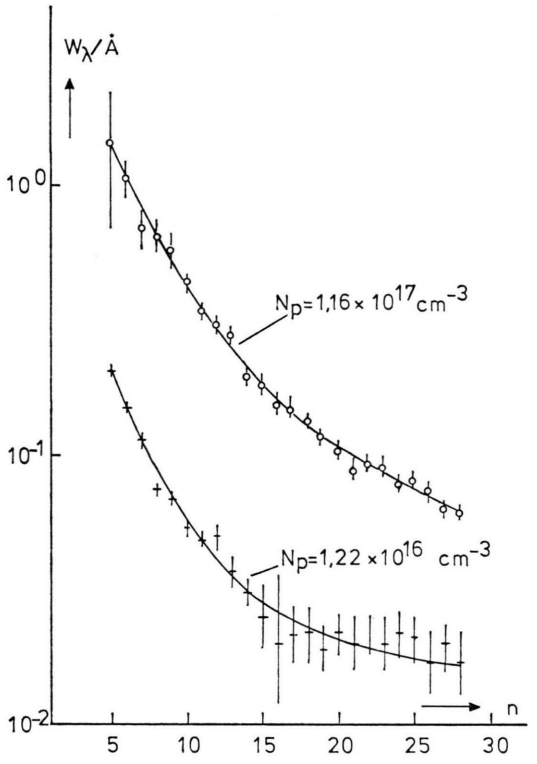

Fig. 5. Total absorption of the Na $3^2S_{1/2} \rightarrow n^2P$ transitions as function of the main quantum number n. $+++++$ measurements at $N_p = 1.22 \times 10^{16}$ cm^{-3}, $T = 701$ K, $l = 34$ cm; ○○○○ measurements at $N_p = 1.16 \times 10^{17}$ cm^{-3}, T = 813 K, $l = 33$ cm.

25% and errors in the value of pressure (2%), temperature (1%) and length of the absorbing layer (3%) obtained from measurement lead to a total statistical error in W_λ of about 15%.

Figures 6 and 7 show that for small n agreement with experiment is much better if 3 – 6-interaction is assumed, whereas for large n the assumption of three-body-interaction leads to better agreement. This was expected, since for large n the latter becomes dominant over binary interaction. From (13) the values of $n_L{}^*$, separating the validity regions of the two types of interaction, are 12 and 18 for the high and the low density, respectively.

Quantitative comparison with the theoretical $W_\lambda(n)$-curves in their respective range of validity shows the following results: At large n there is agreement within error limits. This indicates that the expression (12) for the limiting collisional halfwidth $\Delta\nu_\infty$ is a good approximation. At small n,

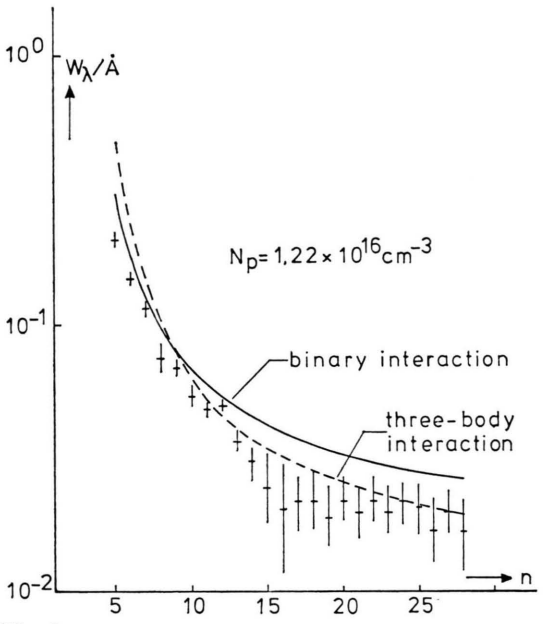

Fig. 6.

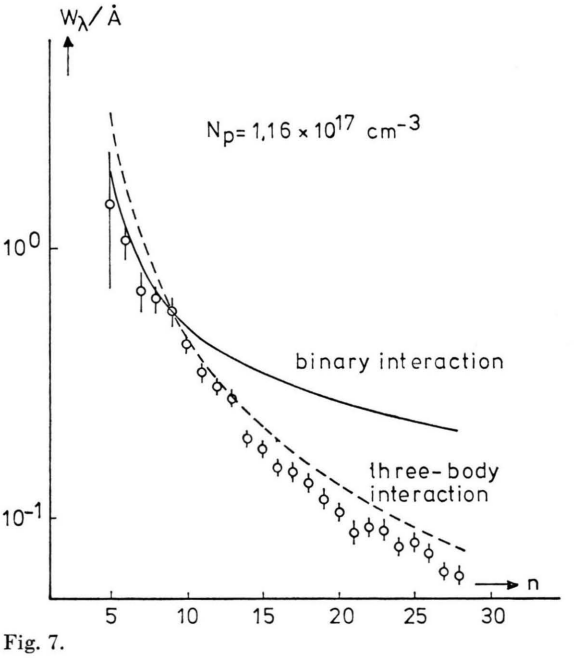

Fig. 7.

Figs. 6, 7. Total absorption of the Na $3^2S_{1/2} \rightarrow n^2P$ transitions as function of the main quantum number. Comparison of experiment and theory. Measurements under same conditions as in Figure 6. ——— calculation assuming binary interaction $V(r) = -C_3 r^{-3} - C_6 r^{-6}$ with resulting collisional halfwidths $\Delta\nu_{3+6}$ taken from Table 1. – – – – calculation assuming three-body-interaction with halfwidths obtained from equn. (12).

on the other hand, the theoretical W_λ-values significantly exceed the experimental ones. The main reason for this deviation does not seem to be the neglect of asymmetries in the line profile in the calculation, since this would yield too small rather than too large W_λ-values. Rather the calculated Lorentz widths seem to be too large. This may be partly due to errors in the calculation of C_6 from (10), (11) and to the neglect of a repulsive term in the assumed binary interaction potential. It is well known [4] that this generally results in too large halfwidths.

For a better understanding of the observed differences measurements of the transmission profiles at higher resolution are clearly desirable. Also, profiles would yield direct information on the interatomic potentials involved. Investigations in this direction are in progress.

[1] Fifth Intern. Conf. Atom. Phys., Berkeley, California 1976.
[2] C. R. Vidal and J. Cooper, J. Appl. Phys. **40**, 3370 (1969).
[3] E. U. Condon and G. H. Shortley, The Theory of Atomic Spectra, Pergamon Press, London 1972.
[4] F. Schuller and W. Behmenburg, Phys. Lett. **12 C**, 275 (1974).
[5] A. W. Ali and H. R. Griem, Phys. Rev. **140 A**, 1044 (1965); Phys. Rev. **144 A**, 366 (1966).
[6] Nat. Bur. Stand. NSRDS-NBS 22, Atomic Transition Probabilities, 1969.
[7] A. Unsöld, Physik der Sternatmosphären, 2. Auflage, Springer-Verlag, Berlin 1968.
[8] R. M. Sternheimer, Phys. Rev. **127**, 1220 (1962).
[9] E. L. Lewis, Proc. Phys. Soc. London **92**, 817 (1967).
[10] C. Reinsberg, Z. Physik **105**, 460 (1937).
[11] P. R. Berman, Appl. Phys. **6**, 283 (1975).
[12] L. Dressler, Diplomarbeit Düsseldorf 1976.
[13] I. I. Sobel'man, Introduction to the Theory of Atomic Spectra, Pergamon Press, London 1972.
[14] T. W. Hänsch, I. S. Shahin, and A. L. Schawlow, Phys. Rev. Lett. **27**, 707 (1971).
[15] T. P. Cotter, Theory of Heat Pipes, Los Alamos, Scientific Report LA-3246-MS (1965).